CERN – EUROPEAN ORGANIZATION FOR NUCLEAR RESEARCH

CLIC – Note – 1139

STRAY MAGNETIC FIELD TOLERANCES FOR THE 380 GEV CLIC DESIGN

Chetan Gohil[1], Daniel Schulte[2], Philip N. Burrows[1]

[1]JAI, University of Oxford, Oxford, United Kingdom
[2]CERN, Geneva, Switzerland

Abstract

The amplitude of external dynamic magnetic fields that can be tolerated by the 380 GeV CLIC design are presented along with the effect of different correction techniques. Different spatial distributions for the magnetic fields are considered. This includes a local magnetic field at a single point, a constant-valued magnetic field across the entire accelerator, a sinusoidal spatial dependence, and a random variation of the magnetic field from point to point.

Geneva, Switzerland
19 November 2018

Stray Magnetic Field Tolerances for the 380 GeV CLIC Design

C. Gohil[1], D. Schulte[2], and P. N. Burrows[1]

[1]JAI, University of Oxford, Oxford, OX1 3PA, United Kingdom
[2]CERN, Geneva, Switzerland

(November 19, 2018)

Abstract

The amplitude of external dynamic magnetic fields that can be tolerated by the 380 GeV CLIC design are presented along with the effect of different correction techniques. Different spatial distributions for the magnetic field are considered. This includes a local magnetic field at a single point, a constant-valued magnetic field across the entire accelerator, a sinusoidal spatial dependence and a random variation of the magnetic field from point to point.

1 Introduction

This paper concerns external (referred to as *stray*) magnetic fields, of which only dynamic magnetic fields are discussed. The temporal variation of the stray field is assumed to be slow enough that the same amplitude is seen across a single bunch train (or *pulse*) of length of 176 ns. It is also assumed that the temporal variation is slow enough that the stray field appears static to a pulse for the duration of 150 μs as it travels through the accelerator. However, the temporal variation does lead to a pulse to pulse variation of the stray field. Such a scenario is valid for frequencies up to a few kHz. The stray field also has a spatial variation, which can be particularly detrimental if it is in resonance with the betatron motion of the beam. Four different spatial models have been considered: *point-like stray fields*, which apply a kick at a single location; *homogeneous stray fields*, which have a constant value across the entire accelerator; *sinusoidal stray fields*, which have a sinusoidal spatial dependence with position along the accelerator and *white noise stray fields*, which vary randomly with position along the accelerator.

Previous studies of sinusoidal stray fields for the 3 TeV CLIC design [1, 2] have shown sensitivities to nT amplitudes and other studies of the 380 GeV design [3] show a similar level of sensitivity. Further simulations of sinusoidal stray magnetic fields in the 380 GeV CLIC design are presented with the effect of different mitigation techniques.

Simulations were performed with the particle tracking code PLACET [4]. To represent the stray field a grid of zero length dipole elements was inserted into the lattice with a spacing of 1 m. The strength of each dipole was set to apply the integrated kick from the stray field over the space between dipoles. The dipoles were used to kick the beam in the vertical direction to simulate the effect of a stray field orientated in the horizontal plane.

The kick from a stray field is related to its amplitude by

$$\delta\ [\mu\text{rad}] = \frac{c \cdot \Delta s\ [\text{m}] \cdot B\ [\text{nT}]}{E\ [\text{GeV}]} \times 10^{-12}, \tag{1}$$

where δ is the dipole kick, c is the speed of light, Δs is the distance between kicks, B is the amplitude of the stray field and E is the energy of the beam.

2 Tolerances

A stray field can lead to luminosity loss in two way: by inducing an offset between the colliding beams at the interaction point (IP) or via emittance growth. The luminosity of two rigid beams colliding with an offset (ignoring the hourglass effect) is given by

$$\mathcal{L} = \frac{N^2 f n_b}{4\pi\sigma_{x,0}\sigma_{y,0}} \exp\left(-\frac{y^2}{4\sigma_{y,0}^2}\right), \tag{2}$$

where N is the number of particles per bunch, f is the repetition frequency, n_b is the number of bunches, $\sigma_{x,0}$ ($\sigma_{y,0}$) is the horizontal (vertical) beam size and y is a vertical offset between them. However, this is equivalent to a collision of two beams with no offset, but with an increased beam size given by

$$\sigma_{y,\text{eff}} = \sigma_{y,0} \exp\left(\frac{y^2}{4\sigma_{y,0}^2}\right). \tag{3}$$

This increase in beam size can be written in terms of emittance as

$$\epsilon_{y,\text{eff}}(y) = \epsilon_{y,0} \exp\left(\frac{y^2}{2\sigma_{y,0}^2}\right) \approx \epsilon_{y,0}\left(1 + \frac{y^2}{2\sigma_{y,0}^2}\right) \approx \epsilon_{y,0} + \Delta\epsilon_{y,\text{eff}}(y), \tag{4}$$

where $\epsilon_{y,0}$ is the ideal vertical emittance and $\Delta\epsilon_{y,\text{eff}}(y) = \epsilon_{y,0} y^2/(2\sigma_{y,0}^2)$ is an effective emittance growth due to the offset. An angle can also be written as an effective emittance growth as

$$\epsilon_{y,\text{eff}}(y') \approx \epsilon_{y,0}\left(1 + \frac{y'^2}{2\sigma_{y',0}^2}\right) \approx \epsilon_{y,0} + \Delta\epsilon_{y,\text{eff}}(y'), \tag{5}$$

where $\Delta\epsilon_{y,\text{eff}}(y') = \epsilon_{y,0} y'^2/(2\sigma_{y',0}^2)$.

To account for the effect of an offset and angle at the end of a section Eqs. (4) and (5) are used to give a total effective emittance growth due to a stray field,

$$\Delta\epsilon_{y,\text{sim}} = (\epsilon_{y,\text{sim}} - \epsilon_{y,0}) + \frac{\epsilon_{y,0} y_\text{sim}^2}{2\sigma_y^2} + \frac{\epsilon_{y,0} y'^2_\text{sim}}{2\sigma_{y'}^2}, \tag{6}$$

where $\epsilon_{y,\text{sim}}$ is the emittance, y_sim is the offset and y'_sim is the angle given by the PLACET simulations with stray fields included.

A 2 % luminosity loss budget is allocated for the effects of stray magnetic fields in the 380 GeV CLIC design. This can be written as an equivalent emittance growth using

$$\mathcal{L} \propto \frac{1}{\sqrt{\epsilon_y}} \implies \frac{\mathcal{L}_0 + \Delta\mathcal{L}}{\mathcal{L}_0} = \sqrt{\frac{\epsilon_{y,0}}{\epsilon_{y,0} + \Delta\epsilon_y}} \implies \Delta\epsilon_y \approx -2\epsilon_{y,0}\frac{\Delta\mathcal{L}}{\mathcal{L}_0}, \tag{7}$$

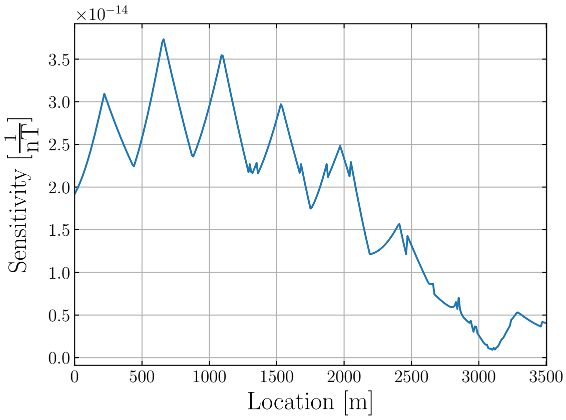

Figure 1: Point sensitivity function of the RTML transfer line.

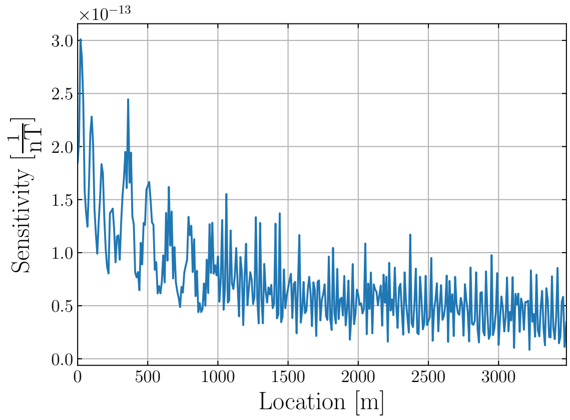

Figure 2: Point sensitivity function of the ML.

where $\mathcal{L}_0$ is the ideal luminosity, $\Delta\mathcal{L}$ is a luminosity loss, $\epsilon_{y,0}$ is the ideal vertical emittance and $\Delta\epsilon_y$ is a vertical emittance growth. Using the nominal value of $\epsilon_{y,0} = 30$ nm in Eq. (7), a vertical emittance growth budget of $\Delta\epsilon_y = 1.2$ nm is obtained.

Tolerances of stray fields were calculated as the amplitude that corresponds to a 1.2 nm emittance growth at the end of a section. The emittance growth due to a stray field scales with the amplitude as

$$\Delta\epsilon_{y,\text{sim}} \propto B^2. \tag{8}$$

Simulations were performed with amplitudes that result in an emittance growth ($\Delta\epsilon_{y,\,\text{sim}}$) a few factors of the budget ($\Delta\epsilon_y \lesssim \Delta\epsilon_{y,\,\text{sim}} \lesssim 3 \cdot \Delta\epsilon_y$). The amplitude used in the simulation is then rescaled with Eq. (8) to calculate the tolerance.

3 Point-Like Stray Fields

A point-like stray field kicks the beam at a single location. Depending on the location of a kick, the effect it can have depends on the beta function, betatron phase and the energy of the beam at that location. A sensitivity function is defined as the emittance growth due to a single kick divided by the amplitude of the kick.

The sensitivity function of the long transfer line in the Ring to Main Linac (RTML), shown in Fig. 1, was found by placing an integrated kick of 1 nT·m at different locations in the transfer line. The sensitivity is proportional to the product of the beta function and phase advance from the location of the kick to the end of the section. The phase advance leads to the long wavelength oscillation of the sensitivity and the beta function leads to the spikes on shorter length scales.

The sensitivity of the Main Linac (ML), shown in Fig. 2, was found by placing an integrated kick of 1 nT·m at different locations in the ML. The regular pattern seen in the sensitivity corresponds to the beta function in the section. The start of the ML is more sensitive due to the lower beam energy.

Two different Beam Delivery System (BDS) designs, which differ in the drift length (L^*) between the final quadrupole and IP, were simulated. The sensitivity of the BDS, shown in Fig. 3, was found by placing an integrated kick of 1 nT·m at different locations in the BDS. Both L^* designs show a virtually identical sensitivity. The most sensitive

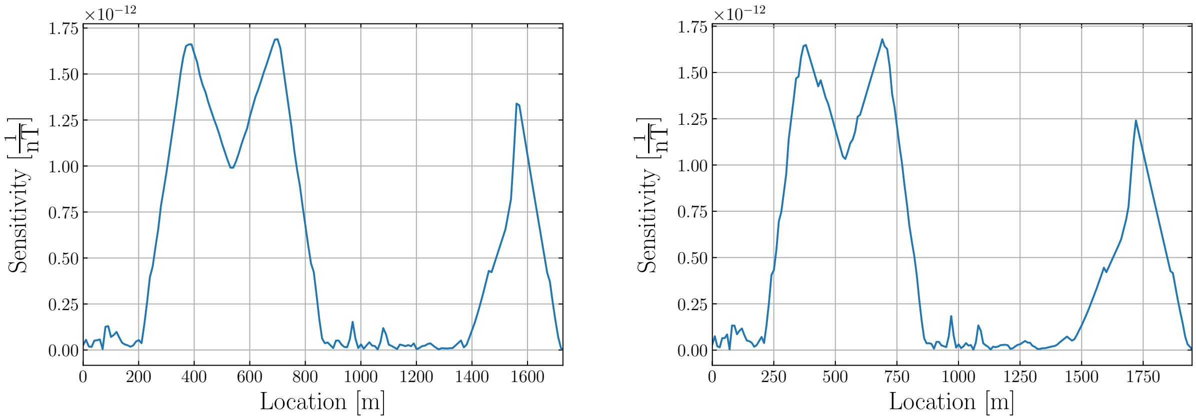

(a) $L^* = 4.3$ m.

(b) $L^* = 6$ m.

Figure 3: Point sensitivity functions of the two BDS designs.

Section(s)	**Tolerance (nT)**
RTML Transfer Line	27
ML	540
ML and BDS ($L^* = 4.3$ m)	1.5
ML and BDS ($L^* = 6$ m)	1.3

Table 1: Tolerance for a 1.2 nm emittance growth from a homogeneous stray field in different sections of CLIC.

locations are those in which a large beta function exists, i.e. in the collimation section and bends before the final focus.

4 Homogeneous Stray Fields

Homogeneous stray fields represent the expected behaviour of typical magnetic field variations from natural sources, such as the Earth's magnetic field, where the variation is homogeneous across the entire accelerator. The tolerances for each section are shown in Tab. 1.

Homogeneous stray fields are symmetric about the IP. This means that any offset due to a stray field will be mirrored by the colliding beams, such that there is no relative offset at the IP. Therefore, tolerances of homogeneous stray fields are from the secondary effect of the stray field to cause emittance growth.

5 Sinusoidal Stray Fields

5.1 Long Transfer Line in the Ring To Main Linac

Any arbitrary spatial distribution of stray fields can be represented as a summation of sine and cosine functions of different wavelengths. Sinusoidal stray fields were simulated to examine the most dangerous wavelengths for CLIC. Stray fields from the accelerator itself, referred to as technical sources, would have a periodic structure, which may be well described with a wavelength approach.

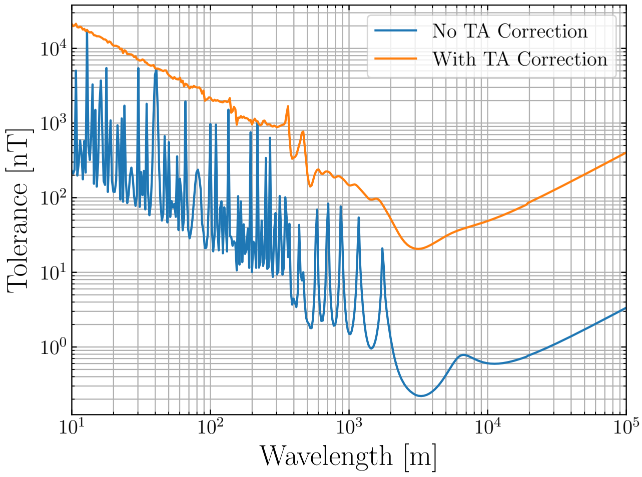

Figure 4: Tolerance for a 1.2 nm emittance growth in the RTML long transfer line, with and without a trajectory correction from a feed-forward mechanism in the turn-around (TA) loop.

The tolerance for a sinusoidal stray field in the long transfer line in the RTML is shown in Fig. 4. A sine function was used to generate the stray field with its origin placed at the start of the transfer line.

The susceptibility to stray fields in the the RTML transfer line is due to the long drifts and relatively weak focusing from the quadrupoles in the line. The minimum tolerance of 0.1 nT corresponds to the stray field wavelength approaching the betatron wavelength of the lattice. The 0.1 nT tolerance therefore corresponds to a worse case scenario where the kicks from the stray field add coherently with the betatron motion.

The RTML contains a turn-around (TA) loop, which provides the possibility of adding a feed-forward mechanism to correct the trajectory of the beam before it enters the ML. Such a scheme would measure the offset of the beam near the start of the TA loop at two locations, which have a phase advance of 90° between them. This enables both the offset and angle of the beam at the end of the TA loop to be fully corrected. The tolerance with a feed-forward mechanism, shown in Fig. 4, indicates that the tolerance can be increased by two orders of magnitude with a perfect trajectory correction applied in the TA.

Whether or not an offset or angle is present at the end of a section depends on the wavelength of the stray field. In some cases, the kicks from the stray field cancel such that there is no final offset or angle. This leads to the periodic structure that is present in the tolerance with no TA correction, where increasing the wavelength results in a larger offset, leading to a tighter tolerance up until a point where increasing the wavelength then acts to reduce the final offset, loosening the tolerance.

5.2 Main Linac and Beam Delivery System

The ML and BDS were integrated into a single simulation. Fig. 5 shows the tolerance for sinusoidal stray fields in the ML and BDS. The origin of the sinusoidal function used to generate the stray fields was placed at the IP. Two types of stray fields have been considered, those which are symmetric about the IP (Cosine) and those which are anti-symmetric about the IP (Sine). Sine-like stray fields introduce a relative offset between the colliding beams at the IP, which is not present for cosine-like stray fields, generally leading to tighter tolerances.

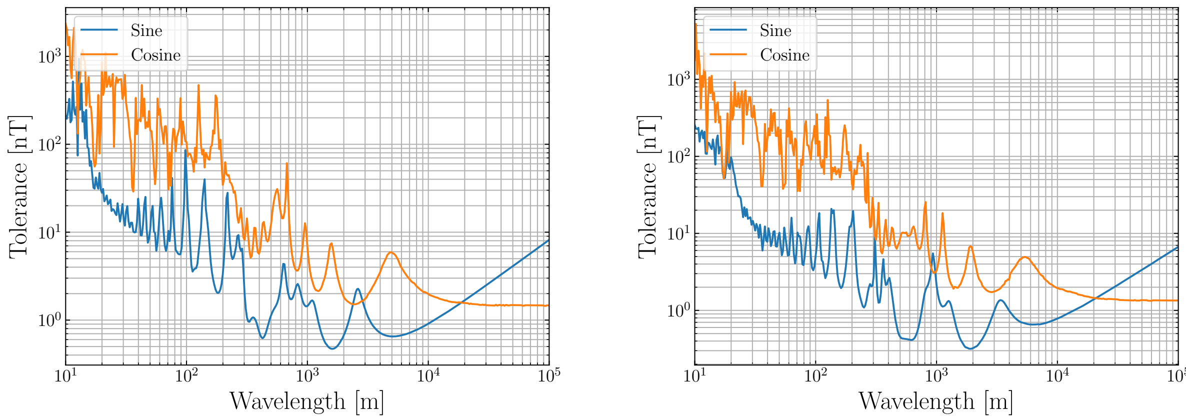

(a) $L^* = 4.3$ m.

(b) $L^* = 6$ m.

Figure 5: Tolerance for a 1.2 nm emittance growth in the ML and BDS.

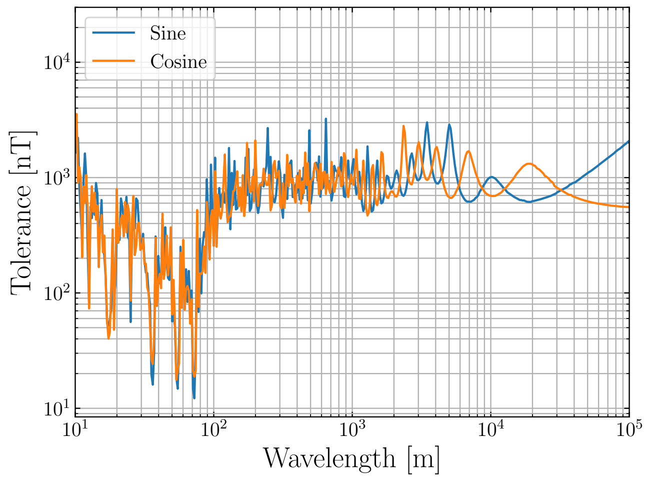

Figure 6: Tolerance for a 1.2 nm emittance growth in the ML and ($L^* = 6$ m) BDS with a perfect shield surrounding the entire BDS beamline.

The minimum tolerance observed in Fig. 5 is approximately 0.1 nT for sine-like stray fields and a tolerance of approximately 1 nT emerges for long wavelength, cosine-like stray fields, which is the expected tolerance from homogeneous stray field simulations.

The effect of surrounding the BDS with a perfect magnetic shield is shown in Fig. 6. This demonstrates that the ML is the most robust section of CLIC with respect to stray fields with tolerances on the order of μT. There will also be an additional benefit in the ML of magnetic shielding provided by the copper walls that form each cavity, suggesting that an effective mitigation strategy can be obtained by targeting just the RTML transfer line and BDS.

The sensitivities at short wavelengths at approximately 20 m, 40 m, 60 m and 80 m correspond to the beta function for different sections of the ML. Comparing the wavelengths that exhibit the tightest tolerances with the spatial lengths of the sensitive regions of the BDS (shown in Fig. 3), it is clear that the tight tolerances in the BDS arise from cases where the stray field is at a maxima in the sensitive regions.

It may be possible to devise an effective strategy to mitigate the effects of stray fields by shielding parts of the BDS opposed to the entire BDS beamline. Fig. 7 shows the

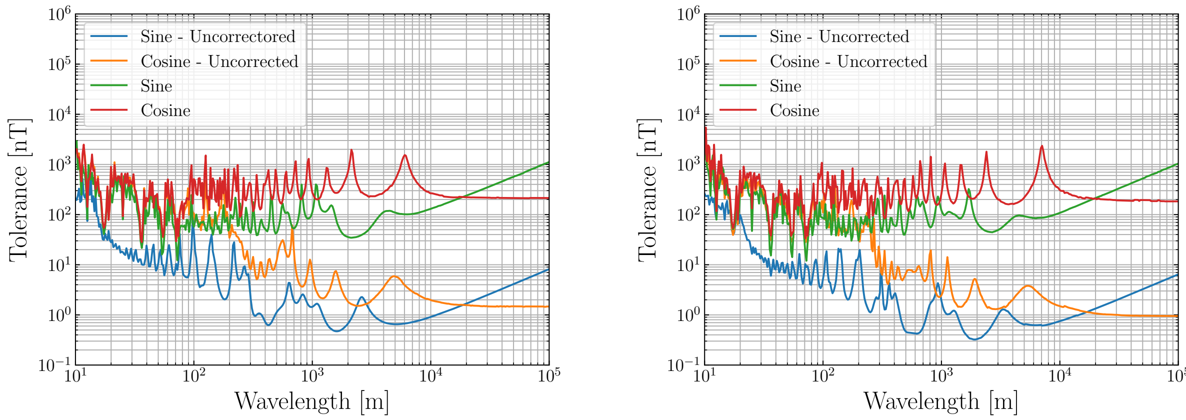

(a) $L^* = 4.3$ m. (b) $L^* = 6$ m.

Figure 7: Tolerance for a 1.2 nm emittance growth in the ML and BDS with a perfect shield surrounding the BDS collimation section and bends before the final focus.

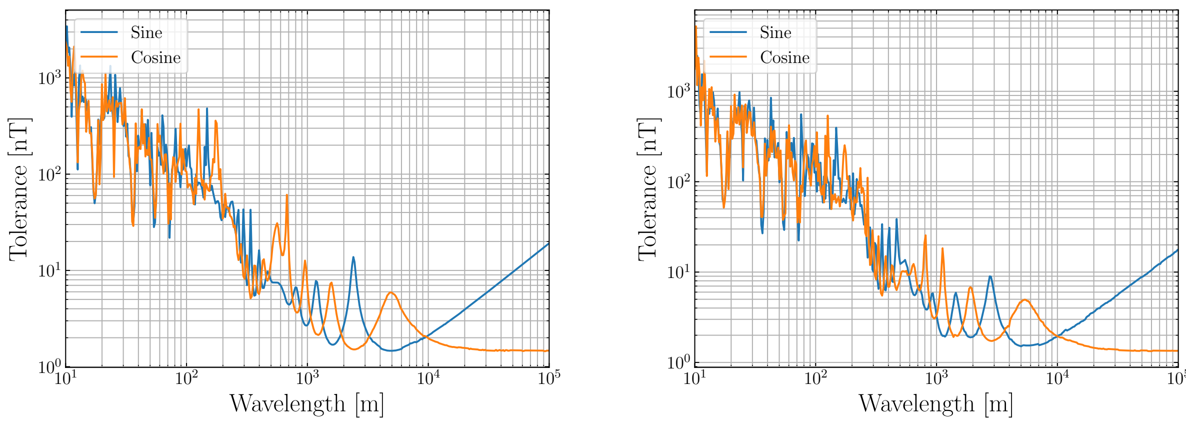

(a) $L^* = 4.3$ m. (b) $L^* = 6$ m.

Figure 8: Tolerance for a 1.2 nm emittance growth in the ML and BDS with a perfect IP feedback system.

tolerance can be increased by an order of magnitude by surrounding just the collimation section and bends before the final focus with a perfect magnetic shield.

The effect of an idealised feedback system that completely removes the relative offset at the IP is shown in Fig. 8. The tolerance can be increased by an order of magnitude with the IP feedback system. The IP feedback system is ineffective for cosine-like stray fields. This is because cosine-like stray fields kick the electron and positron beams in the same direction, ensuring there is no relative offset at the IP. The addition of the IP feedback system also brings the tolerances for sine-like and cosine-like stray fields to the same level, indicating that sine-like and cosine-like stray fields effectively have the same impact on emittance growth and sine-like stray field only seem more important because of the relative offset they induce.

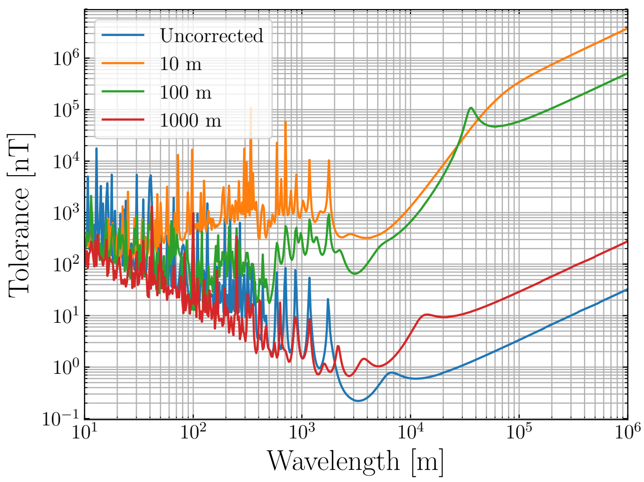

Figure 9: Tolerance for a 1.2 nm emittance growth in the RTML long transfer line with a series of correctors of a particular length placed along the beamline with sensors of the same length. No correction is applied in the TA.

5.3 Stray Field Correctors

A mitigation strategy under consideration is the addition of stray field correctors that would be placed along the beamline to actively compensate the stray fields directly. The effectiveness of such a strategy depends on the granularity of which correctors are placed. For a good correction the length of the correctors must much less than the spatial variation of the stray field.

An active corrector also requires an additional sensor to measure the stray field to be compensated. Two studies have been performed investigating the effect of using sensors of different lengths with the correctors. The first study assumes the length of the sensor is the same as the corrector. Three different sensor/corrector lengths were considered: 10 m, 100 m and 1000 m. The sensors and correctors were placed consecutively along the entire beamline. The correction applied by each corrector was the average stray field measured across the length of the sensor.

Fig. 9 shows the tolerance with a series of correctors in the RTML transfer line. Sensors that measure the stray field over 1000 m would be ineffective as mitigation. This is due to the short wavelength stray fields being averaged over. The 1000 m correctors also appear to reduce the tolerance for short wavelengths. 100 m correctors begin to correct the stray field more effectively and can remove the sensitivity to the betatron wavelength in the transfer line.

Fig. 10 shows the tolerance with a series of correctors with sensors of the same length in the ML and BDS. The addition of the correctors removes the constant tolerance that emerged for long wavelength, cosine-like stray fields. Sensors that measure over a length of 1000 m are ineffective in the ML and BDS.

Another study performed was the effectiveness of using a number of point-like sensors that measure the stray field at one location and use this value to apply a correction to a section of the beamline.

Fig. 11 shows the tolerance in the RTML transfer line with a series of correctors of varying length, with point-like sensors placed at the centre of the region in which the corrector acts. The point-like sensors appear to be more effective at increasing the tolerance for long wavelengths compared to the sensors that span the full length of the correctors.

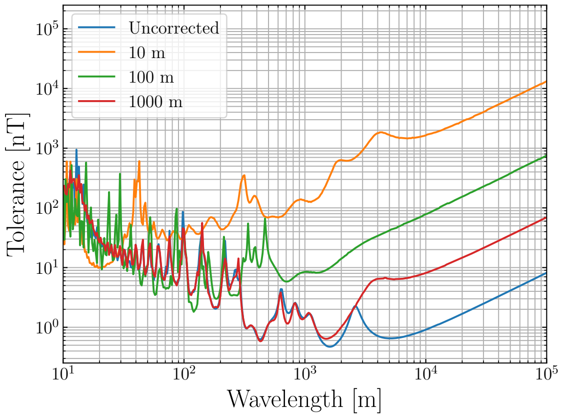

(a) $L^* = 4.3$ m. sine-like.

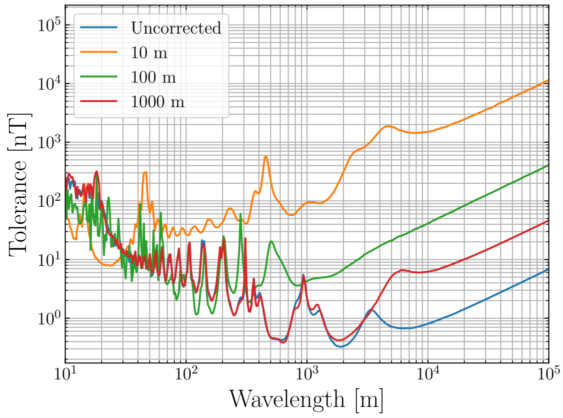

(b) $L^* = 6$ m, sine-like.

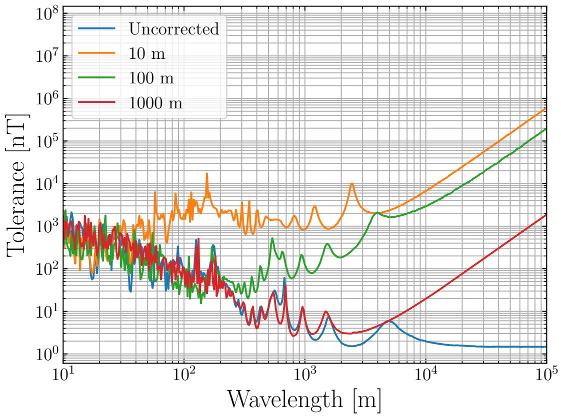

(c) $L^* = 4.3$ m, cosine-like.

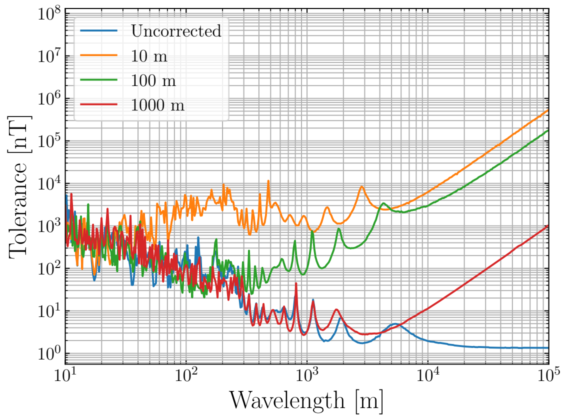

(d) $L^* = 6$ m, cosine-like.

Figure 10: Tolerance for a 1.2 nm emittance growth in the ML and BDS with a series of correctors of a particular length placed along the beamline with sensors of the same length.

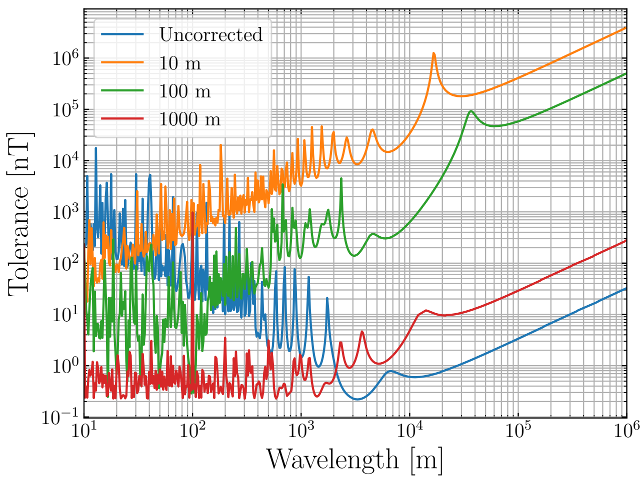

Figure 11: Tolerance for a 1.2 nm emittance growth in the RTML long transfer line with a series of correctors of a particular length placed along the beamline with point-like sensors place at the centre. No correction is applied in the TA.

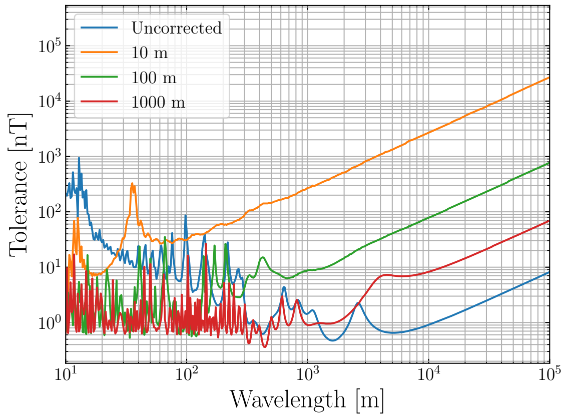

(a) $L^* = 4.3$ m. sine-like.

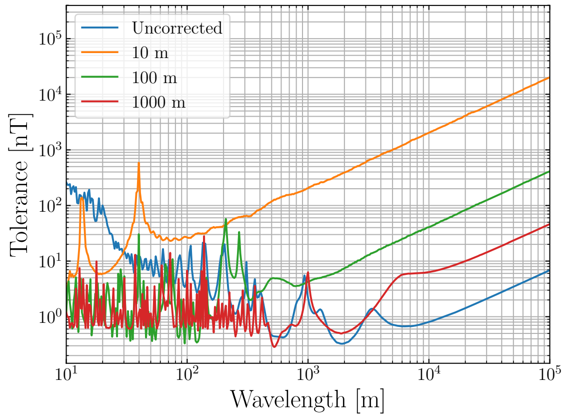

(b) $L^* = 6$ m, sine-like.

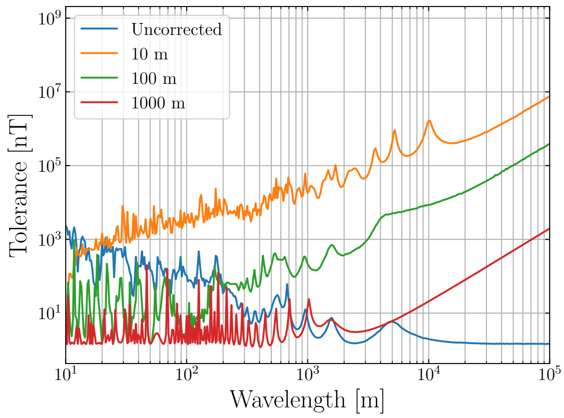

(c) $L^* = 4.3$ m, cosine-like.

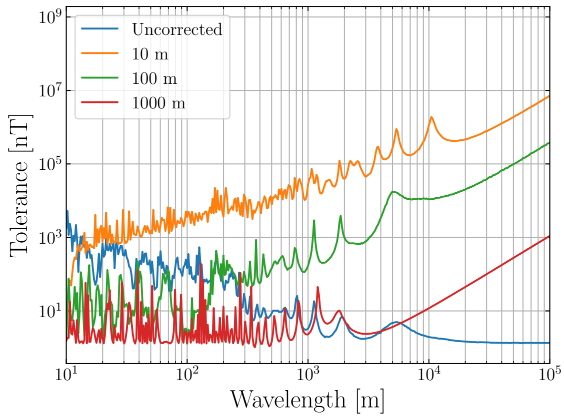

(d) $L^* = 6$ m, cosine-like.

Figure 12: Tolerance for a 1.2 nm emittance growth in the ML and BDS with a series of correctors of a particular length placed along the beamline with a zero length sensor placed at the centre of each corrector.

Section(s)	**Tolerance (nT)**
RTML Transfer Line	10
ML and BDS ($L^* = 4.3$ m)	6.3
ML and BDS ($L^* = 6$ m)	4.9

Table 2: Root-mean-square tolerances that corresponds to a 1.2 nm emittance growth from a Gaussian stray field in different sections of CLIC.

However, the point-like sensors are not effective for short wavelengths. This is due to an over correction that can be applied when the stray field has large fluctions over short distances.

Fig. 12 shows the tolerance in the ML and BDS with a series of correctors of varying length, with point-like sensors placed at the centre of the region in which the corrector acts. Similar to the RTML transfer line, the point-like correctors are more effective for long wavelengths compared to the sensors that span the full length of the correctors, but reduce the tolerance for short wavelengths.

6 White Noise Stray Fields

Stray fields can be characterised in terms of a power spectrum. There is an on-going campaign to measure the power spectrum of stray fields on the CERN site [3]. The kick applied by each dipole was sampled from a Gaussian distribution to examine the effect of a stray field with a white noise power spectrum. This represents a scenario after correction, where each point has been left with some residual stray field from the noise in the corrector. It is not possible to remove this residual noise.

A white noise stray field of power density 1 nT^2/m was simulated 100 times and the emittance growth was averaged. From this the tolerances shown in Tab. 2 were found.

References

[1] J. Snuverink et al., "Impact of Dynamic Magnetic Fields on the CLIC Main Beam", IPAC'10, Kyoto, Japan, May 2010.

[2] E. Marin, D. Schulte, B. Heilig, and J. Pfingstner, "Impact of Dynamical Stray Fields on CLIC", IPAC'17, Copenhagen, Denmark, May 2017.

[3] C. Gohil, P. N. Burrows, E. Marin, D. Schulte, and M. Buzio, "Measurements and Impact of Stray Fields on the 380 GeV Design of CLIC", IPAC'18, Vancouver, BC, Canada, May 2018.

[4] A. Latina et al., "Recent Improvements of the Tracking Code PLACET", EPAC'08, Genoa, Italy, June 2008.